

## Sedimentation of aggregating colloids

Jonathan K. Whitmer<sup>1</sup> and Erik Luijten<sup>2,a)</sup><sup>1</sup>*Department of Materials Science and Engineering and Department of Physics, University of Illinois at Urbana-Champaign, Urbana, Illinois 61801, USA*<sup>2</sup>*Department of Materials Science and Engineering and Department of Engineering Sciences and Applied Mathematics, Northwestern University, Evanston, Illinois 60208, USA*

(Received 8 September 2010; accepted 19 November 2010; published online 20 January 2011)

We investigate the combined effects of gravity, attractive interactions, and Brownian motion in suspensions of colloidal particles and nonadsorbing polymer. Depending on the effective strength of gravitational forces, resulting from a density mismatch between the colloids and the solvent, and the magnitude and range of the depletion interactions induced by the polymer, sedimentation in these suspensions can result in an equilibrium structure or a kinetically arrested state. We employ large-scale molecular dynamics simulations to systematically classify the different regimes that arise as a function of attraction strength and gravitational stress. Whereas strong attractions lead to cluster aggregation and low-density arrested states, moderate attractions can enhance crystallization of the colloidal particles in the sediment. We make direct comparisons to experimental results to infer general conclusions about the mechanisms leading to mechanically stable sediments. © 2011 American Institute of Physics. [doi:10.1063/1.3525923]

### I. INTRODUCTION

The dynamics of colloidal gelation have been studied extensively in experiment and simulation.<sup>1-5</sup> In density-matched suspensions, where the effects of gravity are negligible, continuously increasing the attraction strength between colloids yields first a stable liquid phase of clusters,<sup>1</sup> with homogeneous branched structures forming as attractions are increased further.<sup>2</sup> These clusters can remain suspended, or kinetically arrest to form a gel<sup>1,5</sup> which has a lifetime that depends on colloid concentration and on the presence of long-range repulsive forces (e.g., Coulomb repulsion). Large density mismatches, on the other hand, can give rise to rapid flocculation and sedimentation of clusters before they have time to form a space-spanning network,<sup>6</sup> resulting in an amorphous sediment of clusters. These systems resemble a jammed or glassy state of particle clusters.<sup>7-10</sup> Gravitational stress may also induce particle rearrangement in sediments of weakly attracting colloids by breaking the bonds of particles with few neighbors, thus hindering the formation of an open, gel-like network.<sup>8,11,12</sup> Hence, formation of mechanically stable, gel-like colloidal structures requires either close density-matching to weaken the influence of gravitational forces, or large interparticle attraction strengths.<sup>6</sup>

Gels formed by attractive colloidal particles are interesting from a materials perspective for their ability to support the weight of all other colloids without close-packing. Such mechanical stability is important in, e.g., food processing, where gravity-induced segregation<sup>13,14</sup> of an initially homogeneous dispersion could affect texture and composition. Gel formation can also be an undesirable phenomenon, such as in the manufacturing of colloidal crystals.<sup>15,16</sup> Despite these

applications, the mechanism responsible for formation and stability of low-density gels is relatively poorly understood. Simulation work on sediment formation has focused on regimes where either gravitational strength<sup>17,18</sup> or interparticle attraction strengths<sup>19-21</sup> are very high. In both situations, the contributions to particle dynamics from thermal fluctuations are small, and often ignored. Here, we present a systematic examination of the interplay between interparticle attractive forces and gravitational strength in determining the structure of particle sediments. We focus on systems where thermal fluctuations are not negligible compared to the interparticle attraction and gravitational potential energy scales.

### II. BACKGROUND AND EXPERIMENTAL MOTIVATION

Experiments<sup>22,23</sup> have investigated the structure of sedimenting colloids in the presence of polymeric depletants. Our aim is to determine those suspension properties that result in mechanically stable gels of low density. For comparison between experiment and simulation, it is useful to normalize the strength of attractive forces between colloids and the strength of gravity by the thermal energy scale  $k_B T$ . For gravity, this introduces the dimensionless Péclet number,<sup>23,24</sup>

$$\text{Pe} = \frac{\frac{4}{3}\pi \Delta\rho g a^4}{k_B T}, \quad (1)$$

which characterizes the relative strength of gravitational and thermal stresses on a colloid of radius  $a = \sigma/2$ . Here  $g$  is the gravitational acceleration and  $\Delta\rho$  the density difference between colloid and solvent. Alternative parameters that are sometimes used in place of the Péclet number include the gravitational length  $\xi_g$  and the sedimentation time  $\tau_s$ . Each can be related to the Péclet number by a proper choice of a nondimensionalizing unit. The gravitational length  $\xi_g$  is the

<sup>a)</sup> Author to whom correspondence should be addressed. Electronic mail: luijten@northwestern.edu.

height difference associated with a change  $k_B T$  in gravitational potential energy, so that  $Pe = a/\xi_g$ . In very dilute suspensions of hard-sphere colloids, the gravitational length is the decay constant of the barometric height distribution.<sup>25</sup> The sedimentation time is the time needed for a colloid to freely sediment over its radius, and relates to the Péclet number via the colloidal diffusion time  $\tau_D = a^2/D_s$  by  $Pe = \tau_D/\tau_s$ , where  $D_s$  is the self-diffusion constant of a colloidal particle. The Péclet number thus relates intimately to the dynamics of colloidal particles, as well as their thermodynamic equilibrium state in a gravitational field.

A simple but useful description of a system of colloids in suspension with nonadsorbing polymer is given by the Asakura–Oosawa–Vrij (AOV) model of depletion-induced attraction.<sup>26,27</sup> In this model, the polymer is represented by an ideal gas exerting an osmotic pressure on the colloidal particles. If two surfaces are separated by less than twice the polymer radius of gyration  $R_g$ , polymer coils will be excluded from the volume between the surfaces. Maximization of entropy then drives the surfaces together. The strength of interaction is given by the polymer fraction  $\phi_p = \frac{4}{3}\pi R_g^3/V_{\text{free}}$  within the *free* volume  $V_{\text{free}}$  of the suspension, which in a dilute suspension of colloids is approximately  $V - V_{\text{colloid}}$ , where  $V$  is the total system volume and  $V_{\text{colloid}}$  the volume occupied by the colloids.  $\phi_p$  is also referred to as the *reservoir volume fraction*, as in the dilute colloid limit it corresponds to the polymer concentration in a reservoir in thermodynamic equilibrium with the colloidal suspension. The resulting interaction is controlled by the size ratio  $\zeta \equiv 2R_g/\sigma$  of polymer to colloid,

$$\beta U_{\text{AOV}}(r) = -\phi_p \left( \frac{1+\zeta}{\zeta} \right)^3 \left[ 1 - \frac{3r/\sigma}{2(1+\zeta)} + \frac{1}{2} \left( \frac{r/\sigma}{1+\zeta} \right)^3 \right] \quad \text{for } 1 < r/\sigma < (1+\zeta). \quad (2)$$

Since polymers are treated as ideal in this model, this is only a good approximation if the polymer concentration is small enough that polymer–polymer interactions are irrelevant. Within this regime, the AOV interaction can be tuned over a wide range of attraction strengths by changing  $\zeta$  and  $\phi_p$ . Small size ratios can lead to strong colloidal contact interactions, even at small reservoir fractions.

Experimentally, gels of low volume fraction have been observed in systems with  $\zeta < 0.1$ . In systems of poly(methyl methacrylate) colloids and polystyrene depletant,<sup>22</sup> long-lived structures with a colloid volume fraction  $\phi \lesssim 0.3$  were formed by flocculation and sedimentation. Although the colloids examined were large ( $a \approx 0.63 \mu\text{m}$ ), very slight density mismatching limited the Péclet number of the sediments to  $Pe \approx 0.42$ . Two size ratios,  $\zeta = 1/14$  and  $1/17$ , were examined, each at polymer concentrations that yield an attractive energy  $U_{\text{min}} \approx -4k_B T$  at contact, determined from the minimum of the AOV potential (2). On the other hand, in suspensions of colloidal silica a transition from amorphous, closely packed sediments to a kinetically arrested gel state was observed upon increasing the polymer concentration.<sup>23</sup> In these systems, the large density mismatch increased the Péclet number to  $Pe \approx 2.7$ . The gel states required stronger attractions ( $\approx -8k_B T$ ) to remain stable, due in part to the extra gravitational stress present. However, because a more ex-

treme size ratio ( $\zeta = 0.014$ ) was used than in Ref. 22, this attraction could be achieved at small polymer concentrations.

These experiments hint at the important parameters for controlling gel formation. The volume fraction  $\phi$  determines the frequency of colloidal collisions, and thus influences the rate of cluster formation. The strength  $\beta U$  of each pairwise bond and the permitted relative motion  $\zeta$  of bonded particles directly influence the structure of clusters that form, as well as their yielding behavior. For short-ranged attractive potentials, the second virial coefficient alone determines phase behavior; the precise details of the interparticle potential are unimportant.<sup>28</sup> This central result has recently been applied to gel formation in colloidal suspensions with  $\zeta < 0.1$ ,<sup>3</sup> where the onset of phase separation was found to correspond to the onset of gelation. We therefore expect that, via a suitable mapping, the behavior of systems interacting through a depletion potential can be generalized to systems with other short-range attractions.

### III. MODEL

We simulate the sedimentation of colloidal particles via molecular dynamics (MD) in the constant- $NVT$  ensemble. Brownian motion is controlled via a Langevin thermostat and the presence of nonadsorbing polymer is modeled implicitly via an attractive pair potential. Previous simulations<sup>4,29</sup> combined the depletion interaction (2) with a soft-sphere potential decaying as  $1/r^{36}$  to smoothly define the repulsive particle cores. Furthermore, to ensure that the potential and its first derivative are continuous at the boundary of the attractive region [ $r = (1+\zeta)\sigma$ ], we supplement this potential with a  $1/r^{18}$  term. To make the location of the potential minimum (which defines the center-to-center distance of particles at contact) coincide with  $r = \sigma$ , independent of the depletion strength, a quadratic potential<sup>4</sup> is added piecewise to the model near the colloidal surface. Appropriate proportionality constants guarantee that the potential is smooth everywhere. Defining  $\alpha_2 = (1+\zeta)\sigma$ , we write the resulting pairwise interaction as

$$\beta U(r) = \beta U_{\text{ss}}(r) + \beta U_{\text{att}}(r), \quad (3)$$

where the soft-sphere contribution is given by

$$\beta U_{\text{ss}}(r) = \alpha_1 \left( \frac{1}{r^{36}} - \frac{2}{\alpha_2^{18} r^{18}} + \frac{1}{\alpha_2^{36}} \right) \quad \text{if } r \leq \alpha_2, \quad (4)$$

and the modified depletion interaction by

$$\beta U_{\text{att}}(r) = \begin{cases} B(r-\sigma)^2 + C & \text{if } 0 < r < (1+\alpha_3\zeta)\sigma \\ \beta U_{\text{AOV}}(r) & \text{if } (1+\alpha_3\zeta)\sigma \leq r < \alpha_2. \end{cases} \quad (5)$$

The constants  $B$  and  $C$  follow from continuity of  $\beta U_{\text{att}}$  and its first derivative at  $r = (1+\alpha_3\zeta)\sigma$ ,

$$B = \frac{3\phi_p}{4\alpha_3\zeta^4\sigma^2} ((1+\zeta)^2 - (1+\alpha_3\zeta)^2), \quad (6)$$

$$C = \beta U_{\text{AOV}}(r = \sigma(1+\alpha_3\zeta)) - B(\alpha_3\zeta\sigma)^2. \quad (7)$$

In our simulations we choose  $\alpha_1 = \sigma^{36}$  and set  $\alpha_3$ , which controls the crossover point in Eq. (5), to 0.1.

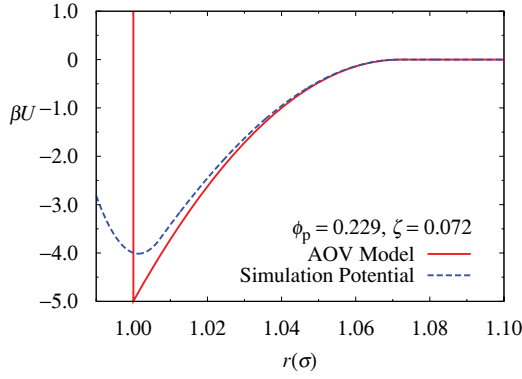


FIG. 1. Comparison of the spatial dependence of the AOV depletion potential (2) and the simulation potential defined in Eqs. (3)–(7). The simulation potential has a shallower minimum than the AOV potential, with a deviation that ranges from  $\mathcal{O}(k_B T)$  for our simulations with polymer–colloid size ratio  $\zeta = 0.072$  to several  $k_B T$  for the simulations with  $\zeta = 0.014$  (cf. Table I). In this figure, we use size ratio  $\zeta = 0.072$  and polymer concentration  $\phi_p = 0.229$ , corresponding to a contact interaction  $U_{\text{AOV}}(r = \sigma)$  of  $-5k_B T$ .

To make contact with Ref. 22, we first choose a size ratio  $\zeta = 0.072$  and vary the polymer volume fraction  $\phi_p$  such that the contact strength of the AOV potential,  $U_{\text{AOV}}^c \equiv U_{\text{AOV}}(r = \sigma)$ , varies from  $-1k_B T$  to  $-7k_B T$ . This allows us to explore a range of potential strengths where thermal effects are relevant. The additional terms in Eq. (3) increase the actual contact energy  $U_{\text{min}}$  by  $\mathcal{O}(k_B T)$  above  $U_{\text{AOV}}^c$ . A representative comparison of the AOV potential and the actual simulation potential is plotted in Fig. 1. Table I provides a full overview of all potential parameters.

Second, in Sec. IV D we examine systems with heavier particles and larger attraction strengths, corresponding to the experiments of Ref. 23. Since the larger attraction strengths are attained through the use of polymer depletants with a more pronounced size asymmetry relative to the colloid, the AOV potential is much steeper, and our choice for the crossover parameter  $\alpha_3 = 0.1$  results in an underestimation of the

TABLE I. Potential energy parameters for the simulations discussed in Sec. IV.  $\beta U_{\text{AOV}}^c$  refers to the strength of the attractive minimum of the ideal hard-sphere AOV model, Eq. (2), and  $\beta U_{\text{min}}$  is the minimum of the actual simulation potential, Eq. (3). Note that a positive value for  $\beta U_{\text{min}}$  implies repulsion at contact. The top part of the table refers to the simulations discussed in Secs. IV A–IV C, whereas the bottom part of the table refers to those discussed in Sec. IV D.

$\beta U_{\text{AOV}}^c$	$\zeta$	$\alpha_2/\sigma = 1 + \zeta$	$\phi_p$	$B$	$C$	$\beta U_{\text{min}}$
-1	0.072	1.072	0.045	1692.057	-0.088	-0.375
-3			0.137	5151.374	-0.267	-2.186
-5			0.229	8160.691	-0.446	-3.996
-7			0.321	12070.009	-0.626	-5.806
0	0.014	1.014	0.000	0.000	0.000	0.510
-8			0.076	376785.787	-7.399	-7.131
-12			0.111	550305.558	-10.806	-10.539
-18			0.167	827937.190	-16.258	-15.991
-24			0.222	1100611.115	-21.612	-21.345
-36			0.333	1650916.673	-32.419	-32.151

attractive contact energy. This difference can be as much as  $4k_B T$  for the strongest attractions studied (cf. Table I).

Some earlier simulations<sup>4</sup> have included a repulsive barrier,  $k_B T$  in height, to prevent macroscopic liquid–gas phase separation. The mathematical form of this potential is given by

$$\beta U_{\text{barrier}} = A \left[ \left( \frac{2\sigma - r}{2\sigma - \alpha_2} \right)^4 - 2 \left( \frac{2\sigma - r}{2\sigma - \alpha_2} \right)^2 + 1 \right] \quad \text{if } \alpha_2 < r < 2\sigma. \quad (8)$$

This term is added to the particle potential  $\beta U(r)$  beyond the cutoff radius  $\alpha_2$ , and due to its form is smooth at both  $r = \alpha_2$  and  $r = 2\sigma$ . The resulting potential favors the formation of small clusters and gel-like networks by rendering next-nearest neighbor interactions repulsive and thus limiting aggregation to certain orientations of pairwise contacts.<sup>4</sup> We perform simulations both with and without this barrier by setting  $A = 1$  or  $A = 0$ .

All simulations consist of 3380 particles sedimenting in an elongated rectangular cell of dimension  $14.8\sigma \times 14.8\sigma \times 44.6\sigma$ , resulting in a global colloid volume fraction  $\phi = 0.181$ . We set the unit length to  $\sigma$ , the unit mass to  $M_c$ , and the unit energy to  $k_B T$ , thus defining a unit thermal velocity  $v_{\text{th}} = \sqrt{k_B T/M_c}$ . The drag coefficient in the Langevin thermostat is set to  $13.2\xi_c$ , where  $\xi_c = \sqrt{k_B T M_c}/\sigma$  is the unit of friction. Periodic boundaries are imposed in the  $x$  and  $y$  directions, whereas a smooth shifted-truncated 9–3 Lennard-Jones wall is utilized to enforce boundaries in the  $z$ -direction,

$$\beta U_{\text{wall}}(\Delta z) = \varepsilon \left[ \frac{2}{15} \left( \frac{\sigma_w}{\Delta z} \right)^9 - \left( \frac{\sigma_w}{\Delta z} \right)^3 + \frac{\sqrt{10}}{3} \right] \quad \text{if } \Delta z < \left( \frac{2}{5} \right)^{1/6} \sigma_w. \quad (9)$$

Here  $\Delta z$  denotes the distance of a colloid from the wall and we choose the parameters  $\sigma_w = 3\sigma$  and  $\varepsilon = 15$ . Gravity is applied along the  $-z$  direction, with its strength chosen to achieve Péclet numbers in the range 0.054 to 0.537. All dispersions start from randomly determined homogeneous conditions.

Our simulations utilize velocity-Verlet integration<sup>30</sup> to evolve colloidal trajectories. Within this scheme, the molecular dynamics time step  $\Delta t_{\text{MD}}$  must be chosen small enough that attractive interactions are accurately explored. A maximum time step criterion can be derived by requiring that a colloid in a single time step traverses a typical distance  $\Delta x = v_{\text{th}} \Delta t_{\text{MD}} \ll \zeta \sigma$ . We choose  $\Delta t_{\text{MD}} = 7.07 \times 10^{-5} t_c$  with  $t_c = \sigma/v_{\text{th}}$ , which for our choices of  $\zeta$  satisfies this criterion easily. Such a small time step necessarily means that dispersions will evolve very slowly from a uniform distribution of particles to a stable sediment, especially at the lowest values of gravitational force. This slow evolution limits the number of particles that can be examined in a simulation. Consequently, our sediments have a thickness of only 10 to 15 diameters when closely packed. Nevertheless, we are able to observe various general trends.

We note that these simulations ignore several effects that may be of importance in nonequilibrium solid formation, such

as particle–particle friction, particle–wall friction,<sup>31</sup> and hydrodynamic interactions.<sup>32,33</sup> This allows us to concentrate on the interplay between the interparticle depletion potential and gravitational stress. Since particles that interact via a central potential are inherently smooth, no mechanical stability in the sediment can arise from friction considerations. Any kinetic arrest in the sediments is thus a direct result of interparticle forces.

Previous simulations that couple aggregation with sedimentation have been performed for lattice-bound particles in the Diffusion-Limited Cluster Aggregation (DLCA) limit,<sup>34,35</sup> as well as for off-lattice particles interacting via the Derjaguin–Landau–Verwey–Overbeek (DLVO) potential combined with an adhesion potential.<sup>19–21</sup> These earlier models differ from the current study in that they treat bonds as irreversible. In the DLCA systems, this corresponds to an effectively infinitely strong static friction, since two particles cannot change their relative position once they have come into contact. For the DLVO-based model, clusters still exhibit a small degree of deformability through reorientations that are permitted as long as the participating particles have few enough contacts. Nevertheless, the effective particle friction is still very high. We note that the effect of finite particle friction in combination with adhesive (van der Waals) forces has been examined for granular particles,<sup>17,18</sup> but such studies are fundamentally different from the simulations presented here since they do not include the effects of thermal fluctuations. A noteworthy point about the simulations of Refs. 19 and 20 is that they incorporated hydrodynamic interactions. At low Péclet number, these interactions were found to not have a strong effect on the final sediment structure. At moderate Péclet numbers most comparable to our simulations, very loosely packed structures ( $\phi \approx 0.1$ ) were obtained. However, we observe that this may have been caused by two important differences compared to our simulations: First, the assumption of irreversible aggregation, which prevents the reorientation of particles relative to each other and hence counteracts densification of the sample under the influence of gravity. Second, these earlier studies did not examine cluster formation of particles prior to sedimentation. We find that this process has a significant effect on the final density of the sediment for our largest attraction strengths  $|U_{\text{AOV}}^c| > 5k_B T$ .

The pioneering simulations of Ref. 36 examined suspensions of particles interacting via both purely repulsive and attractive square-well potentials in sedimentation equilibrium. These simulations utilized Monte Carlo moves and were incapable of probing the metastable gel and glass states resulting from the kinetic arrest of the constituent particles. It was observed that a gravitational field can induce segregation of particles into different phases, allowing the observation of phase coexistence in sedimentation equilibrium, where osmotic pressure and gravitational forces balance. Since the pressure experienced by particles in the sediment varies continuously as a function of their vertical position within the sediment, this yields a cross-section of the phase diagram. Phase coexistence manifests itself as a region over which the density changes abruptly with height.<sup>37,38</sup> It must be emphasized that this is only valid for systems that are in thermal equilibrium. Moreover, equilibrium phases are strictly only

defined for slices with a thickness  $h \ll \xi_g$ , so that the pressure remains constant within the slice.

## IV. RESULTS AND DISCUSSION

### A. Sedimentation profiles and radial distribution functions

As noted above, the presence of a gravitational potential permits simultaneous access to multiple density regions of the phase diagram of colloidal suspensions, provided that interparticle forces are sufficiently weak to avoid a kinetically arrested state. To inform our understanding of the sediment structure, it is useful to note which regions of the phase diagram are sampled by our simulations. Owing to the short attraction range, we expect to observe at most two coexisting phases,<sup>39</sup> unlike the square-well fluid of Ref. 36 which exhibits three distinct phases as a function of height and pressure. Thus, as the gravitational force is increased, an equilibrium crystalline structure is expected at the bottom of the cell.

In Fig. 2, we plot density profiles obtained in our simulations. We consider four different attraction strengths (cf. top part of Table I) and six values for the gravitational acceleration. Each curve is averaged over the resultant configurations from five independent runs, i.e., with different, randomly determined initial conditions. The runs are continued until the sediments are mechanically stable and do not compact further. A sediment is considered stable if the centroid of all colloids does not move more than one colloidal radius in height over several hundred sedimentation times  $\tau_s$ . For small Péclet numbers, sedimentation is very slow and it takes  $\mathcal{O}(10^8)$  MD steps to reach this state. In addition, we find that the colloidal structures remain mobile over long time scales. Sediments experience slow compaction and abrupt, rare rearrangements, where the motion of individual particles or clusters allows sedimentation to proceed to an energetically more favorable state.

From the averaged density profiles, we can draw some general conclusions about the sediment structure. For small attraction strengths [ $\beta U_{\text{AOV}}^c = -1$  in Fig. 2(a) and  $\beta U_{\text{AOV}}^c = -3$  in Fig. 2(b)], systems behave as if in equilibrium. At  $\text{Pe} = 0.054$ , colloidal particles form a fluid phase whose density increases gradually toward the bottom of the sample. This tendency increases as the gravitational strength is increased. At these small attraction strengths, thermal fluctuations are likely to break colloidal contacts, so that increasing the Péclet number acts to densify the sediment. For  $\beta U_{\text{AOV}}^c = -3$  [Fig. 2(b)] this leads to quite striking behavior when  $\text{Pe} > 0.194$ , where the particles experience enhanced ordering at the bottom of the cell, yielding very well-defined layers whose densities suggest a close-packed solid. Although one might expect kinetic trapping to play a role for attraction strengths greater than  $k_B T$ , our simulations show that moderate attractions enhance crystal formation, rather than hinder it.

As we increase the attraction strength, [ $\beta U_{\text{AOV}}^c = -5$  in Fig. 2(c) and  $\beta U_{\text{AOV}}^c = -7$  in Fig. 2(d)], we observe irregular concentration profiles resulting from porous structures that increase in density as the Péclet number is increased. The stronger attractions limit the relative motion of colloids,

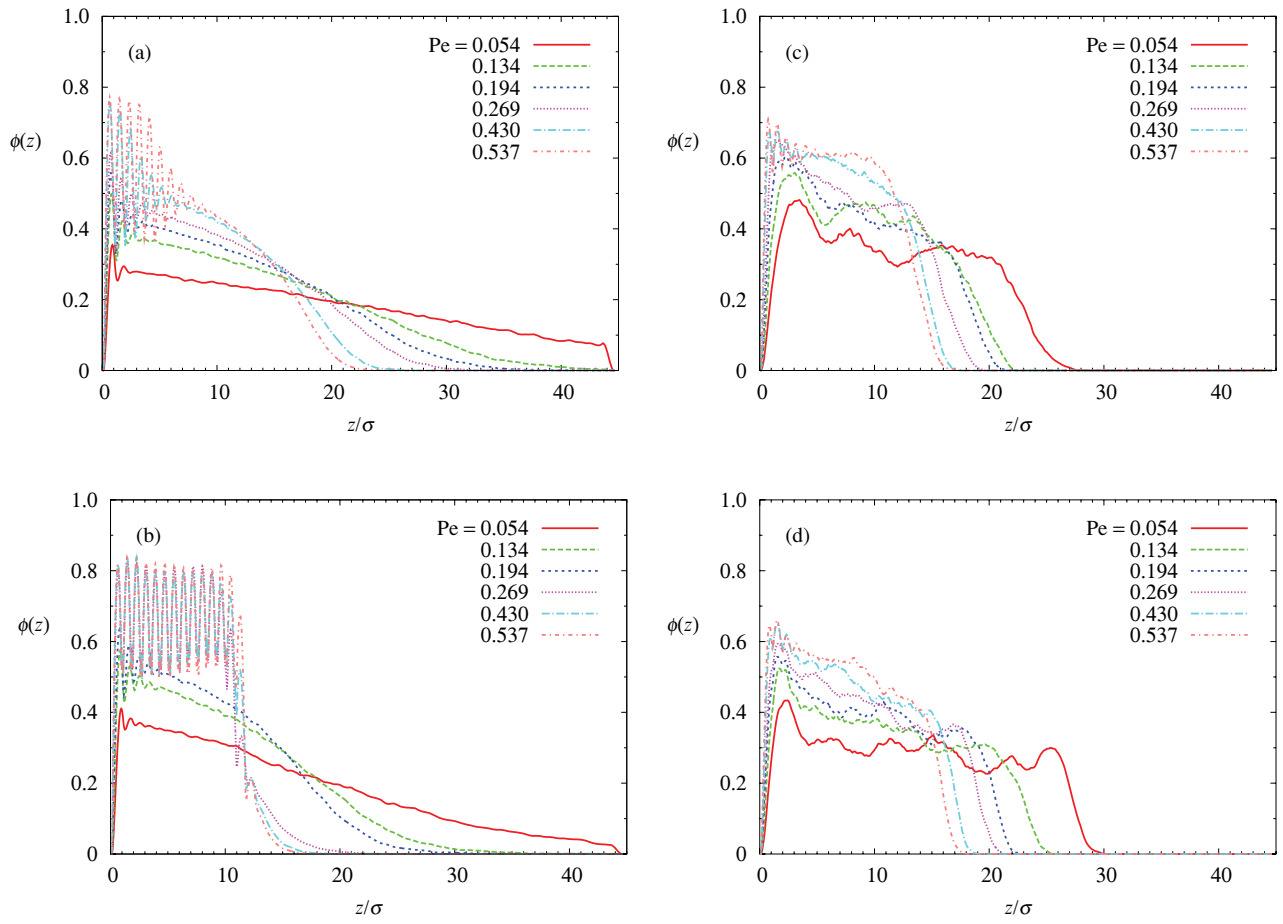


FIG. 2. Colloid volume fraction as a function of distance from the bottom wall of the sample cell for the systems described in Sec. IV A. Gravitational force is varied in each plot via the Péclet number  $Pe$ . The panels pertain to different attraction strengths as measured in terms of the contact value of the AOV potential, Eq. (2): (a)  $\beta U_{AOV}^c = -1$ ; (b)  $\beta U_{AOV}^c = -3$ ; (c)  $\beta U_{AOV}^c = -5$ ; (d)  $\beta U_{AOV}^c = -7$ . The precise potential parameters for these simulations are in given Table I. Large gravitational forces induce strong layering at the bottom of the cell, which is initially enhanced by attractive forces [cf. panels (a) and (b)].

causing them to form dense clusters. The combined effects of attraction and cluster formation tend to decrease the density of particle sediments. Tightly packed structures formed during sedimentation do not break up and rearrange into an equilibrium solid upon reaching the bottom of the cell, but instead settle into a mechanically stable state. As a result, structures are highly ordered over a few particle diameters, but disordered at length scales beyond the typical cluster size.

To obtain more detailed information about the sediment structures, we also examine the local structure around a colloidal particle via the radial distribution function  $g(r)$  (Fig. 3). To minimize the influence of surface-induced crystallization in the bottom layers and a lack of neighbor particles near the top of the sediment, the radial distribution function is only computed for colloids residing between  $z = 5\sigma$  and  $z = 15\sigma$ . In some of the samples, notably the solidlike sediments of Fig. 2(b), there is significant density variation over this range in  $z$ . However, in those cases the computed  $g(r)$  is weighted heavily by the dense particle packings near the bottom and should not be strongly affected by the upper layers. Also, at high Péclet number, the gravitational length  $\xi_g$  becomes small ( $\xi_g = \sigma$  at  $Pe = 0.537$ ), so that the pressure varies over a wide range within the slab employed for the calculation of  $g(r)$ . However, for high  $Pe$  the sediment density

tends to be high and relatively insensitive to the pressure; consequently  $g(r)$  does not vary appreciably over the slab in these cases.

Combining the results for the density profiles and the radial distribution function, we now systematically discuss the behavior of the colloidal sediments. For  $\beta U_{AOV}^c = -1$ , the attractive interaction between the colloid is very weak and since the global volume fraction of the colloids is only 0.181, a homogeneous fluid phase would be expected in the absence of gravity. However, with increasing Péclet number dense layers arise near the flat bottom of the sample cell, as revealed by the density profiles [Fig. 2(a)]. Since this dense regime lies mostly outside the averaging window of  $g(r)$  the radial distribution function [Fig. 3(a)] remains largely structureless. When the colloidal attraction is increased to  $\beta U_{AOV}^c = -3$ , the system remains in the fluid state if  $Pe \lesssim 0.194$ . This fluid is more dense than observed for  $\beta U_{AOV}^c = -1$ , resulting in a steeper fall-off in the density profiles [Fig. 2(b)], but the only change in  $g(r)$  is a stronger peak at contact [Fig. 3(b)]. However, for  $Pe \geq 0.269$ ,  $g(r)$  develops strong peaks out to separations of  $4\sigma$ . The sharp nearest and next-nearest neighbor peaks are located at the positions expected for close packing and reconfirm the onset of a crystalline phase for moderate attraction strength, as inferred above from the density profiles.

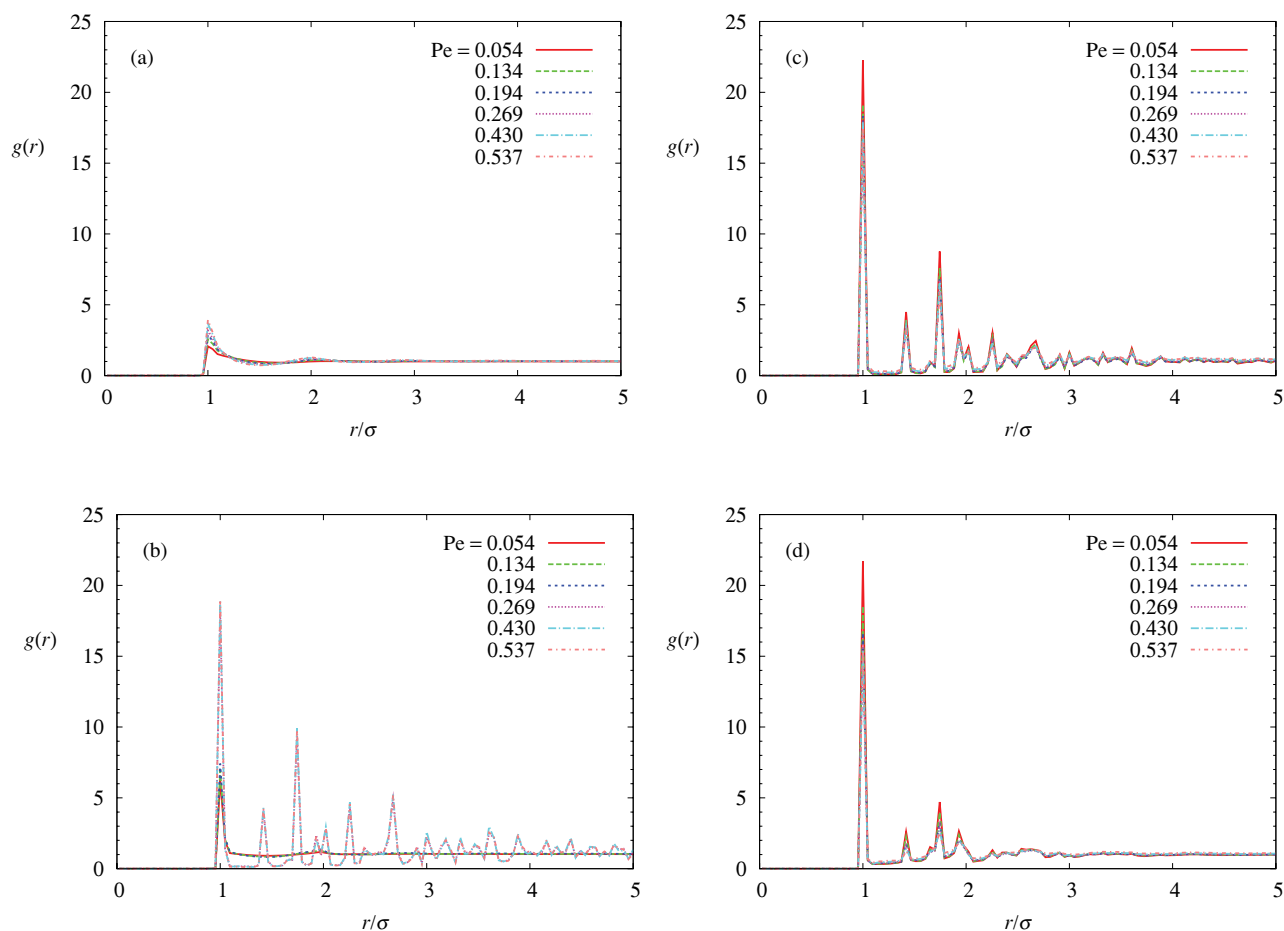


FIG. 3. Radial distribution function  $g(r)$  for attractive colloidal particles in mechanically stable sediments as a function of gravitational acceleration. Each panel represents a different attraction strength: (a)  $\beta U_{\text{AOV}}^c = -1$ ; (b)  $\beta U_{\text{AOV}}^c = -3$ ; (c)  $\beta U_{\text{AOV}}^c = -5$ ; (d)  $\beta U_{\text{AOV}}^c = -7$ . For discussion, see the text.

Qualitatively different behavior emerges as attractions are further increased to  $\beta U_{\text{AOV}}^c = -5$ . For  $\text{Pe} = 0.054$ , the density profile [Fig. 2(c)] shows a loosely packed sediment ( $\phi \approx 0.4$ ), which however retains a radial distribution [Fig. 3(c)] similar to those found in the crystal-like packings for  $\beta U_{\text{AOV}}^c = -3$  [Fig. 3(b)]. This suggests that during sedimentation tightly packed clusters form, and that jamming of these clusters results in an arrested state that is mechanically stable at relatively low volume fractions. Although attraction strength and range here are comparable to those in experiment (e.g., Ref. 22), we observe sediment densities a factor of two larger. This may be attributed in part to greater translational freedom in our potential compared to the AOV potential, which may result in greater rearrangements of pairwise contacts. The fact that even at our largest attraction strength, larger Péclet numbers result in denser sediments than seen in experiment indicates that the mechanism of kinetic arrest in the experimental gels is due to more than the interparticle potential energy alone, and that frictional surface contacts<sup>17</sup> or hydrodynamic forces<sup>32</sup> may play a role. Increasing gravitational strength leads to more compact sediments. At  $\text{Pe} = 0.537$ , the volume fraction of the sediment away from its upper and lower boundaries is a near-uniform 0.6. This value is very similar to that of random close-packing, and suggests a sediment that is more glassy than gel-like. The radial

distribution function [Fig. 3(c)] is largely unchanged and continues to show ordering peaks over a range of  $3\sigma$ , indicating that the sediment is formed by an incongruous packing of crystalline clusters, rather than by random arrangement of the spheres themselves.

Finally, at the highest attraction strength [ $\beta U_{\text{AOV}}^c = -7$ , Fig. 2(d)], more porous sediments are created. At the lowest Péclet number, the average sediment density in the region  $z > 5\sigma$  is  $\phi \approx 0.3$ , although fluctuations of  $\pm 0.05$  remain observable even after averaging. The packing density increases as the Péclet number is increased, but for all profiles remains below the highest packing density observed for  $\beta U_{\text{AOV}}^c = -5$ . Also, for all values of  $\text{Pe}$ ,  $g(r)$  now shows ordering of the sediment only within a particle separation  $2\sigma$  [Fig. 3(d)]. This indicates that the stronger attraction leads to the formation of clusters with a lower degree of ordering. This illustrates that, whereas attraction strength determines much of the local structure in colloidal sediments, the sedimentation rate and gravitational stresses defined by the Péclet number have significant effects on the final structures.

To address the role of crystallization, we repeat all calculations with an additional repulsive barrier in the colloidal pair potential, Eq. (8). At  $\beta U_{\text{AOV}}^c = -1$  the behavior of the samples [see Fig. 4(a)] is only weakly dependent on the presence of this barrier, and also  $g(r)$  (not shown) only shows a slightly

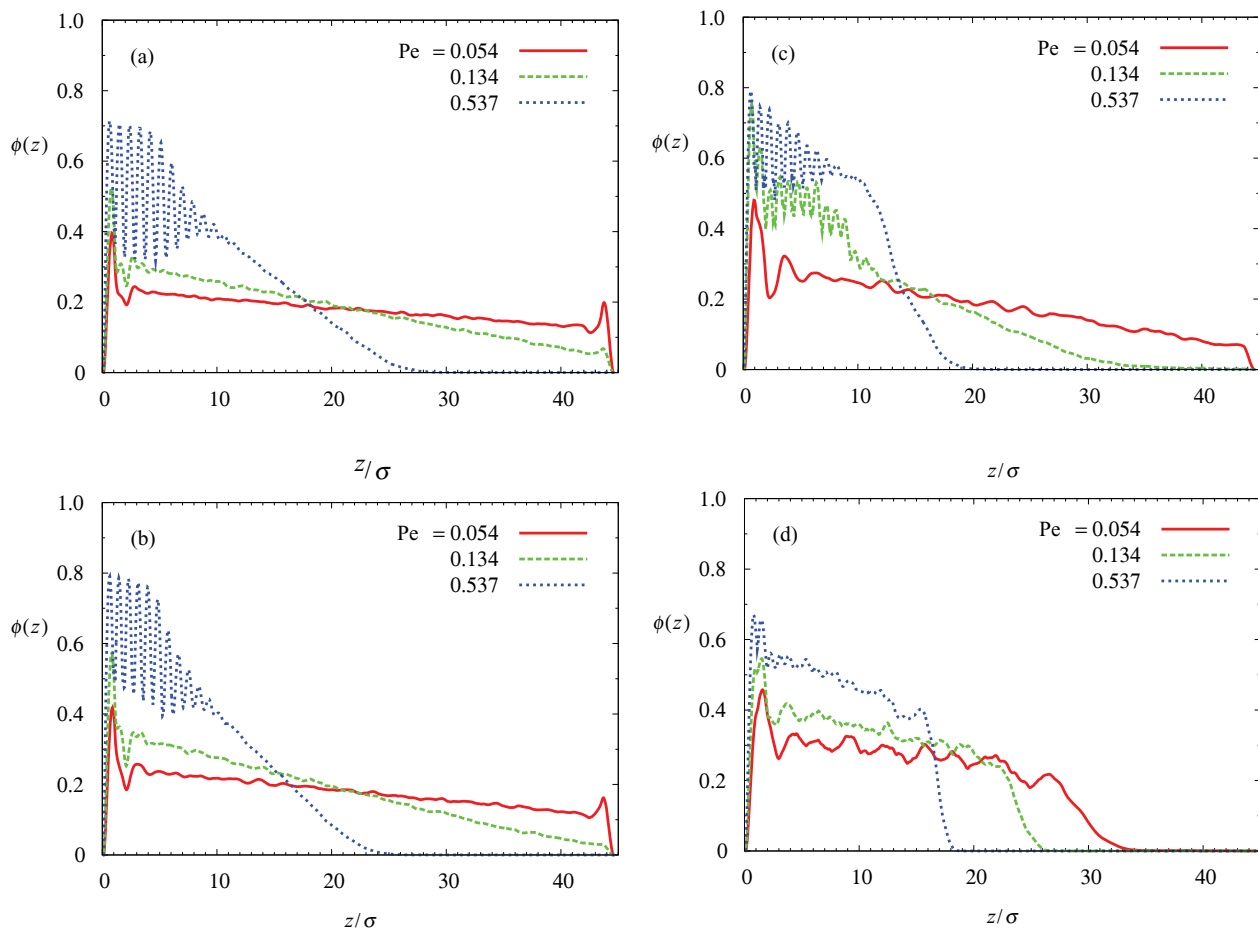


FIG. 4. Colloid volume fraction as a function of the distance from the bottom wall of the sample cell for systems in which a repulsive barrier, Eq. (8), has been added to the colloidal interaction. Gravitational force is varied in each plot via the Péclet number  $Pe$ . The panels pertain to different attraction strengths as measured in terms of the contact value of the AOV potential, Eq. (2): (a)  $\beta U_{AOV}^c = -1$ ; (b)  $\beta U_{AOV}^c = -3$ ; (c)  $\beta U_{AOV}^c = -5$ ; (d)  $\beta U_{AOV}^c = -7$ . For discussion see the text.

reduced peak at contact. At  $\beta U_{AOV}^c = -3$ , however, the frustration brought on by the repulsive barrier markedly changes the sediments for larger Péclet number [cf. Fig. 4(b)], with the uniform layering persisting only a few layers before giving way to liquidlike ordering. Interestingly, at  $\beta U_{AOV}^c = -5$ , the sedimentation profiles in the presence of a barrier [Fig. 4(c)] are completely different from those in Fig. 2(c). Low Péclet numbers yield a more uniform density across the entire sample while high Péclet numbers show stronger layering than simulations without the barrier, albeit with a lower density than in Fig. 4(b). The layer formation is almost completely absent at  $\beta U_{AOV}^c = -7$  [Fig. 4(d)], but compared to Fig. 2(d) the additional repulsion leads to a significant decrease in the sediment density at low Péclet numbers.

## B. Osmotic pressure

In sedimenting systems, osmotic pressure is related to local volume fraction via the force-balance equation

$$\Pi(\phi(z)) = \int_z^\infty \Delta \rho g \phi(z') dz'. \quad (10)$$

Integration of the density profiles in Fig. 2 allows us to obtain the local osmotic pressure and investigate how its den-

sity dependence changes with increasing attraction strength (Fig. 5). This relation has been used in experiments to determine the equation of state of both hard-spherelike<sup>37</sup> and attractive<sup>38</sup> colloids. In addition, the osmotic pressure can provide an indication of the volume fraction at which a gel becomes mechanically stable. At this point, kinetically arrested particles will resist further compaction, leading to a steep increase in osmotic pressure as a function of sediment volume fraction.

At small attraction strengths, the pressure shows little dependence on gravity. For  $\beta U_{AOV}^c = -1$  [Fig. 5(a)], all curves coincide, in accordance with our interpretation that these systems are in or near equilibrium. The slight deviation of the curve for  $Pe = 0.054$  originates from the presence of the wall at the top of the system—for larger gravitational strengths the colloidal particles are insensitive to this wall. The fluidlike portions of these curves align closely with the Carnahan–Starling equation of state for hard spheres,<sup>40</sup> but lie slightly below it owing to the attraction between the particles. The oscillations in  $\Pi(\phi)$  that arise once the volume fraction reaches approximately 50% simply are an artifact resulting from the occurrence of layers in the sediment. To render the  $\phi \rightarrow z$  mapping unique, the concentration should be averaged over at least a full layer. We note that the layer formation

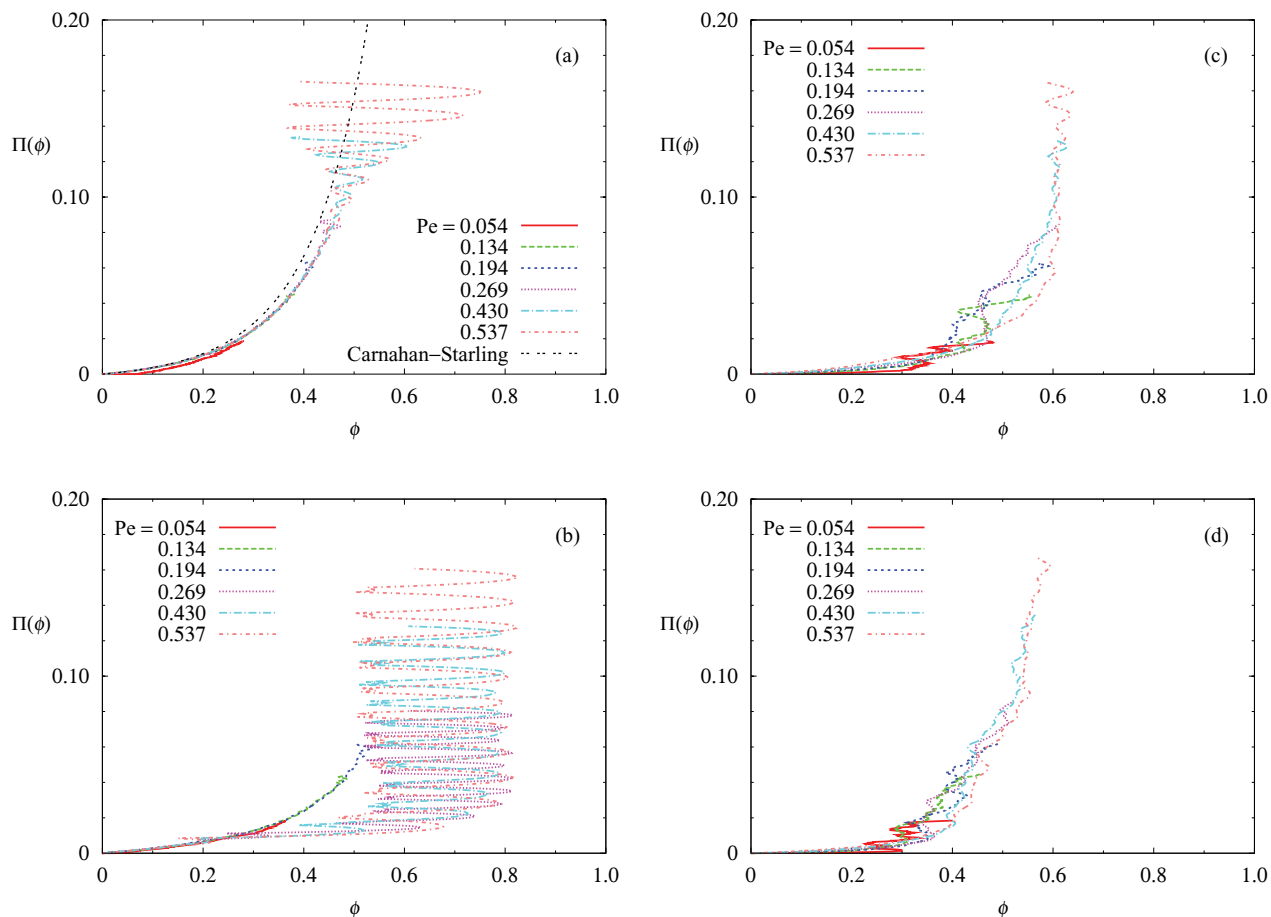


FIG. 5. Equation of state (osmotic pressure  $\Pi$  as a function of local colloid volume fraction  $\phi$ ) for attractive particle sediments obtained by integrating the density profiles in Fig. 2. The panels pertain to different attraction strengths: (a)  $\beta U_{AOV}^c = -1$ ; (b)  $\beta U_{AOV}^c = -3$ ; (c)  $\beta U_{AOV}^c = -5$ ; (d)  $\beta U_{AOV}^c = -7$ . For discussion see text. In panel (a), the Carnahan–Starling equation of state for a hard-sphere liquid (Ref. 40) is plotted for comparison.

roughly agrees with the onset of liquid–solid phase separation in a hard-sphere fluid. For stronger attractions, this coexistence region will widen,<sup>41</sup> and the results for  $\beta U_{AOV}^c = -3$  [Fig. 5(b)] are in agreement with the appearance of a relatively dense solid at high pressures. However, due to the finite height of our samples, at the highest Péclet numbers almost all particles participate in the solid phase. This makes it difficult to distinguish true phase coexistence.

As the attraction is increased from  $-1k_B T$  to  $-3k_B T$ , the pressure required to reach a certain sediment density *decreases*. For stronger attractions,  $\beta U_{AOV}^c = -5$  [Fig. 5(c)] and  $\beta U_{AOV}^c = -7$  [Fig. 5(d)], however, this trend reverses, which is another indicator of gel formation. Namely, once a gel has formed, large forces are necessary to break the interparticle bonds providing mechanical stability and compact the sediment. This is also consistent with the observation that the osmotic pressure in Figs. 5(c) and 5(d) increases steeply at lower volume fractions than in Figs. 5(a) and 5(b).

### C. Bond number distribution

The bond number  $N_{\text{bond}}$  for each particle is another indicator of the local packing structure, and thus can elucidate the factors leading to kinetic arrest. Systems that undergo gelation or jamming tend to have a smaller number

of neighbors per particle than close-packed crystals.<sup>23,42</sup> We define particles to be bonded if their center-to-center distance is less than the range of the depletion attraction,  $(1 + \zeta)\sigma$ , and plot histograms of the bond number taken over the entire sample in Fig. 6. These data strongly support the conclusions of the previous sections. For  $\beta U_{AOV}^c = -1$  [Fig. 6(a)] most particles do not have any bonds at  $Pe = 0.054$ . As the Péclet number is increased the average bond number increases monotonically, but remains less than six, confirming that all systems are primarily in the fluid state. When the attraction is increased to  $\beta U_{AOV}^c = -3$  [Fig. 6(b)], low-Pe dispersions exhibit a similar structure, but for  $Pe = 0.269$  a strong peak arises at  $N_{\text{bond}} = 12$ , indicating a close-packed structure. The particles with less than 12 neighbors correspond to crystalline defects or boundary layers. Thus, under sufficient gravitational stress colloidal attraction enforces a dense structure. The bond-number distribution does not change significantly as  $Pe$  is increased further, suggesting that the structure cannot be densified further by gravity.

For stronger attractions, a completely different behavior emerges. The packing for  $\beta U_{AOV}^c = -5$  [Fig. 6(c)] retains a clear peak at  $N_{\text{bond}} = 12$ , but the distribution also shows an increased probability for structures that are not close-packed, with a secondary maximum around  $N_{\text{bond}} = 8$ . This is consistent with a sediment composed of kinetically arrested clusters.

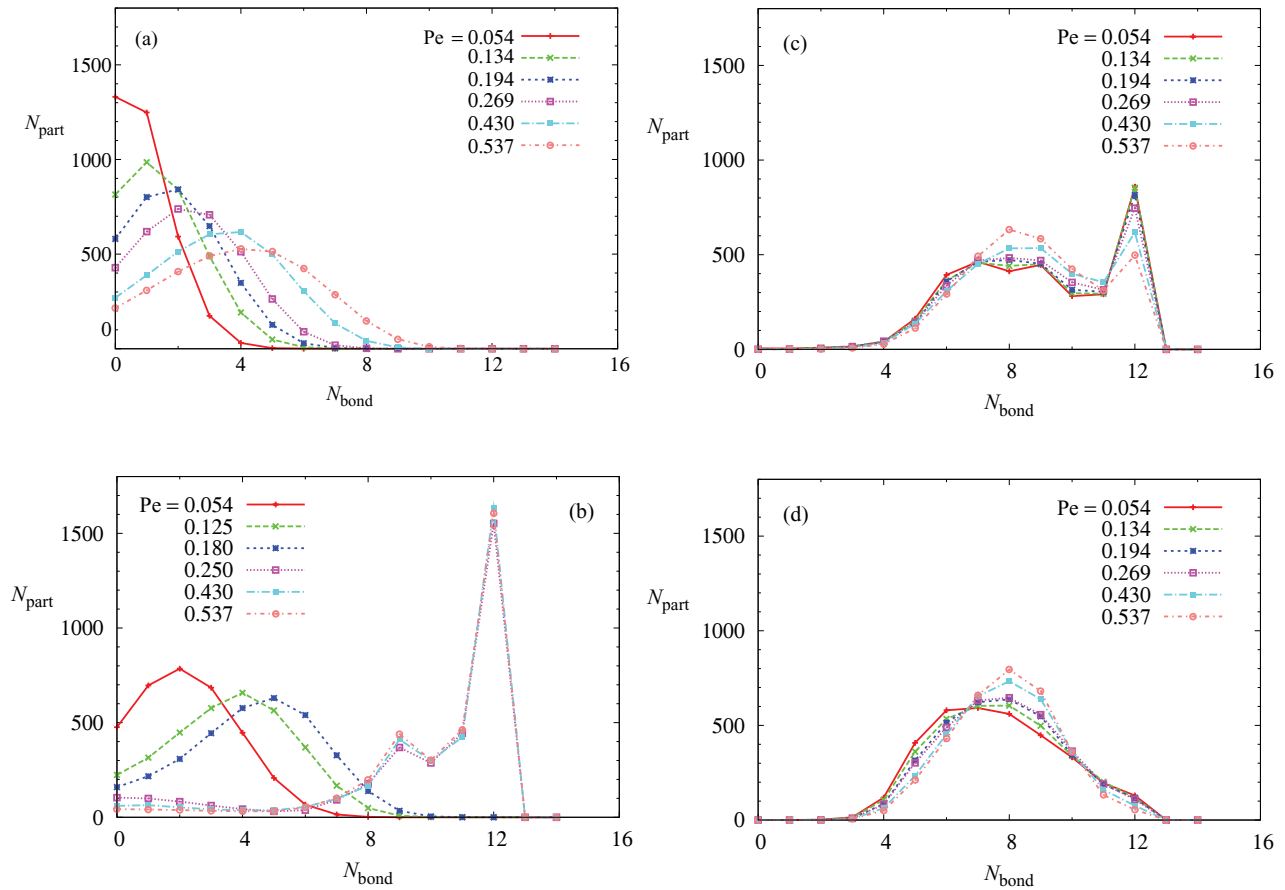


FIG. 6. Bond number distributions for attractive colloidal particles in sediment as a function of gravitational acceleration and attraction strength: (a)  $\beta U_{\text{AOV}}^c = -1$ ; (b)  $\beta U_{\text{AOV}}^c = -3$ ; (c)  $\beta U_{\text{AOV}}^c = -5$ ; (d)  $\beta U_{\text{AOV}}^c = -7$ . Two particles are defined to be in contact if their center-to-center distance is within the range of the depletion attraction, Eq. (2).

Particles at the centers of these clusters have coordination numbers similar to particles in a bulk solid, but those at the cluster surface have fewer bonds, similar to particles in a glassy or liquid state. The resultant structure will have a lower average density due to voids between the dense-packed clusters. Although, for this attraction, the sediment density displays significant dependence on gravitational strength, the bond number distribution varies only relatively weakly with Péclet number. Furthermore, the highest values for  $Pe$ , which yield the most dense sediments, display a *lower* average bond number. One explanation is that at lower  $Pe$  particles have more time to rearrange into close-packed structures during sedimentation. This interplay between sedimentation and particle rearrangement suggests that hydrodynamic interactions between the colloids could play a significant role. However, in the present simulations there is merely a competition between the time scales for sedimentation and nucleation. Lastly, at  $\beta U_{\text{AOV}}^c = -7$ , the bond distribution [Fig. 6(d)] shifts toward still smaller values. The attraction is now so strong that bonded particles are unable to rearrange into an optimal packing before new particles are added to the cluster. As a result, the peak at  $N_{\text{bond}} = 12$  disappears, in agreement with the absence of any layer formation in Fig. 2(d).

#### D. Strong binding regime

To connect to the results of Ref. 23, we repeat a subset of the sedimentation runs for colloids with a stronger attractive

potential of shorter range,  $\zeta = 0.014$ . All parameters for the interaction potential are listed in Table I. The Péclet number is fixed at  $Pe = 2.7$ . As illustrated in Fig. 7, the sediment density decreases monotonically with increasing attraction strength, reaching values as low as  $\phi \approx 0.3$ , with only a slight increase near the wall due to surface-induced ordering.

The bond number distributions (Fig. 8) confirm the open structure, with a peak around  $N_{\text{bond}} = 6$ , and are similar to those reported experimentally (cf. Fig. 8 in Ref. 23). We note

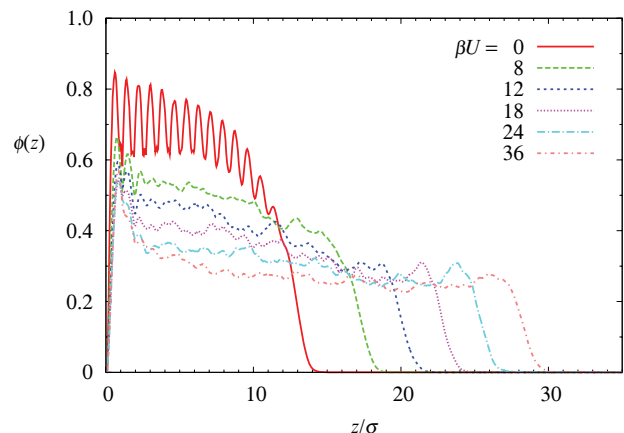


FIG. 7. Density profiles of sediments with a Péclet number of 2.7 in the strong binding regime, representing the experiments of Ref. 23.

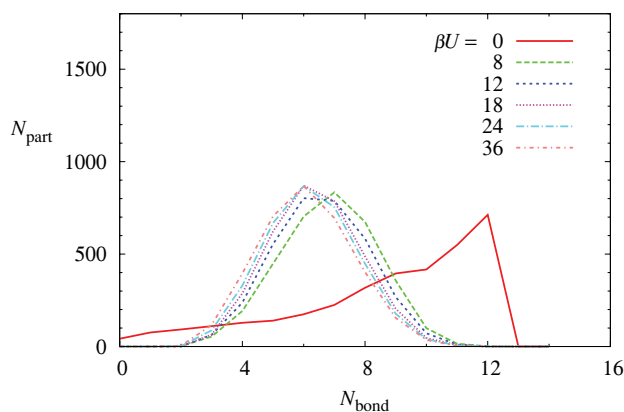


FIG. 8. Bond number for sediments with Péclet number  $Pe = 2.7$  in the strong binding regime.

the marked shift compared to the bond number distributions found in Sec. IV C for suspensions of colloids experiencing a larger attraction range, at considerably lower Péclet number [cf. Fig. 6(d)]. On the other hand, the distributions in Fig. 8 change only very weakly with increasing attraction strength (for  $\beta U_{AOV}^c > 0$ ), whereas the experiments observe a marked decrease in the average bond number (with a peak in the distribution around  $N_{\text{bond}} = 4$ ) upon addition of polymer. It is likely that in these tightly bound systems surface friction between particles becomes more important,<sup>43,44</sup> rendering a sediment more mechanically stable than it would be with central forces alone.<sup>17</sup> Furthermore, the initial (global) volume fraction  $\phi = 0.181$  used here is higher than in the experiments.<sup>23</sup> Since this influences the rate of cluster formation during sedimentation, it could be an additional factor in the lower sensitivity of the bond number distribution to the depletion strength.

## V. CONCLUSION

In summary, we have examined the interplay of colloidal attractions and gravitational forces in determining the structure of particle sediments. We find that for interaction strengths that are too low to induce cluster formation during sedimentation, the density profiles of the colloidal sediment are very similar to those expected for equilibrium colloidal suspensions, with gravitational forces acting to densify the phase present at the bottom of the sample cell. Furthermore, modest attraction strengths are found to enhance the growth of crystalline phases, rather than inhibit them. When the attraction strength is increased still further, dense colloidal clusters form during sedimentation, which settle into loosely packed, disordered structures. Our simulations reproduce various experimentally observed features of colloidal sedimentation, although in the case of larger ranges of the depletion potential we need significantly stronger attractions than required in experiment to achieve open structures. Possible causes for this difference are the omission of interparticle friction and hydrodynamic interactions between colloids. Studies to incorporate these effects are currently underway.

## ACKNOWLEDGMENTS

This material is based upon work supported by the National Science Foundation under Grant Nos. DMR-0346914 and DMR-1006430.

- <sup>1</sup>P. J. Lu, J. C. Conrad, H. M. Wyss, A. B. Schofield, and D. A. Weitz, *Phys. Rev. Lett.* **96**, 028306 (2006).
- <sup>2</sup>C. J. Dibble, M. Kogan, and M. J. Solomon, *Phys. Rev. E* **74**, 041403 (2006).
- <sup>3</sup>P. J. Lu, E. Zaccarelli, F. Ciulla, A. B. Schofield, F. Sciortino, and D. A. Weitz, *Nature* **453**, 499 (2008).
- <sup>4</sup>A. M. Puestas, M. Fuchs, and M. E. Cates, *Phys. Rev. E* **67**, 031406 (2003).
- <sup>5</sup>F. Sciortino, S. Mossa, E. Zaccarelli, and P. Tartaglia, *Phys. Rev. Lett.* **93**, 055701 (2004).
- <sup>6</sup>H. Sedgwick, S. U. Egelhaaf, and W. C. K. Poon, *J. Phys.: Condens. Matter* **16**, S4913 (2004).
- <sup>7</sup>V. Trappe, V. Prasad, L. Cipelletti, P. N. Segrè, and D. A. Weitz, *Nature* **411**, 772 (2001).
- <sup>8</sup>P. N. Segrè, V. Prasad, A. B. Schofield, and D. A. Weitz, *Phys. Rev. Lett.* **86**, 6042 (2001).
- <sup>9</sup>K. Kroy, M. E. Cates, and W. C. K. Poon, *Phys. Rev. Lett.* **92**, 148302 (2004).
- <sup>10</sup>J. M. Valverde, M. A. S. Quintanilla, and A. Castellanos, *Phys. Rev. Lett.* **92**, 258303 (2004).
- <sup>11</sup>D. Senis and C. Allain, *Phys. Rev. E* **55**, 7797 (1997).
- <sup>12</sup>J. R. Weeks, J. S. van Duijneveldt, and B. Vincent, *J. Phys.: Condens. Matter* **12**, 9599 (2000).
- <sup>13</sup>R. Buscail, *Colloids Surf.* **5**, 269 (1982).
- <sup>14</sup>C. Kim, Y. Liu, A. Kühnle, S. Hess, S. Viereck, T. Danner, L. Mahadevan, and D. A. Weitz, *Phys. Rev. Lett.* **99**, 028303 (2007).
- <sup>15</sup>W. Lee, A. Chan, M. A. Bevan, J. A. Lewis, and P. V. Braun, *Langmuir* **20**, 5262 (2004).
- <sup>16</sup>C. J. Martinez, J. Liu, S. K. Rhodes, E. Luijten, E. R. Weeks, and J. A. Lewis, *Langmuir* **21**, 9978 (2005).
- <sup>17</sup>K. J. Dong, R. Y. Yang, R. P. Zou, and A. B. Yu, *Phys. Rev. Lett.* **96**, 145505 (2006).
- <sup>18</sup>R. Y. Yang, R. P. Zou, A. B. Yu, and S. K. Choi, *Phys. Rev. E* **78**, 031302 (2008).
- <sup>19</sup>G. C. Ansell and E. Dickinson, *J. Chem. Phys.* **85**, 4079 (1986).
- <sup>20</sup>E. Dickinson, *J. Colloid Interface Sci.* **118**, 286 (1987).
- <sup>21</sup>J.-F. Li, C.-S. Chen, B.-Y. Yu, and W.-C. J. Wei, *J. Am. Ceram. Soc.* **89**, 1257 (2006).
- <sup>22</sup>Y. Gao and M. Kilfoil, *J. Phys.: Condens. Matter* **16**, S5191 (2004).
- <sup>23</sup>M. H. Lee and E. M. Furst, *Phys. Rev. E* **74**, 031401 (2006).
- <sup>24</sup>S. Ramaswamy, *Adv. Phys.* **50**, 297 (2001).
- <sup>25</sup>J. Perrin, *Ann. Chim. Phys.* **18**, 1 (1909).
- <sup>26</sup>S. Asakura and F. Oosawa, *J. Chem. Phys.* **22**, 1255 (1954).
- <sup>27</sup>A. Vrij, *Pure Appl. Chem.* **48**, 471 (1976).
- <sup>28</sup>M. G. Noro and D. Frenkel, *J. Chem. Phys.* **113**, 2941 (2000).
- <sup>29</sup>J. J. Cerdà, T. Sintès, C. M. Sorensen, and A. Chakrabarti, *Phys. Rev. E* **70**, 051405 (2004).
- <sup>30</sup>M. P. Allen and D. J. Tildesley, *Computer Simulation of Liquids* (Clarendon, Oxford, 1987).
- <sup>31</sup>J.-M. Condro, C. Ligoure, and L. Cipelletti, *J. Stat. Mech.* **2007**, P02010 (2007).
- <sup>32</sup>H. Tanaka and T. Araki, *Phys. Rev. Lett.* **85**, 1338 (2000).
- <sup>33</sup>P. N. Segrè, F. Liu, P. Umbanhowar, and D. A. Weitz, *Nature* **409**, 594 (2001).
- <sup>34</sup>A. E. González, *J. Phys.: Condens. Matter* **14**, 2335 (2002).
- <sup>35</sup>A. E. González, *Phys. Rev. E* **74**, 061403 (2006).
- <sup>36</sup>T. Biben, J.-P. Hansen, and J.-L. Barrat, *J. Chem. Phys.* **98**, 7330 (1993).
- <sup>37</sup>M. A. Rutgers, J. H. Dunsmuir, J.-Z. Xue, W. B. Russel, and P. M. Chaikin, *Phys. Rev. B* **53**, 5043 (1996).
- <sup>38</sup>S. Buzzaccaro, R. Rusconi, and R. Piazza, *Phys. Rev. Lett.* **99**, 098301 (2007).
- <sup>39</sup>M. Dijkstra, J. M. Brader, and R. Evans, *J. Phys.: Condens. Matter* **11**, 10079 (1999).
- <sup>40</sup>N. F. Carnahan and K. E. Starling, *J. Chem. Phys.* **51**, 635 (1969).
- <sup>41</sup>M. Dijkstra, R. van Roij, and R. Evans, *Phys. Rev. E* **59**, 5744 (1999).
- <sup>42</sup>R. Y. Yang, R. P. Zou, and A. B. Yu, *Phys. Rev. E* **62**, 3900 (2000).
- <sup>43</sup>H. Yoshizawa, Y. L. Chen, and J. Israelachvili, *J. Phys. Chem.* **97**, 4128 (1993).
- <sup>44</sup>E. M. Furst and J. P. Pantina, *Phys. Rev. E* **75**, 050402(R) (2007).